OPEN

Nanostructured Zr-Pd Metallic Glass Thin Film for Biochemical Applications

Sergey V. Ketov[1], Xuetao Shi[1], Guoqiang Xie[2], Ryotaro Kumashiro[1], Alexander Yu. Churyumov[3], Andrey I. Bazlov[3], Na Chen[1,4], Yoshifumi Ishikawa[1,5], Naoki Asao[1], Hongkai Wu[1] & Dmitri V. Louzguine-Luzgin[1]

[1]WPI Advanced Institute for Materials Research, Tohoku University, Aoba-Ku, Sendai 980-8577, Japan, [2]Institute for Materials Research, Tohoku University, Aoba-Ku, Sendai 980-8577, Japan, [3]National University of Science and Technology "MISiS", Moscow, Russia, [4]School of Materials Science and Engineering, Tsinghua University, Beijing 100084, P. R. China, [5]Department of Chemistry, Graduate School of Science, Tohoku University, Sendai 980-8578, Japan.

Zr-Pd metallic glassy thin films with a hierarchical nano-scale structure, produced by magnetron sputtering of the Zr and Pd powder mixture, demonstrate a unique combination of physical and biochemical properties. Thermal stability of the nano-structured glassy samples, their resistance to oxidation in dry air and phase transformation behavior are discussed in the present work. These binary alloy samples also show exceptionally high corrosion resistance and spontaneous passivation in a simulated body fluid. Experiments on the catalytic activity and biocompatibility of this nanostructured metallic glass indicate that this is a very suitable material for biochemical applications. Compared to the multicomponent alloys studied earlier this binary alloy has much simpler chemical composition, which makes preparation of the sample with defined stoichiometry easier, especially when the elements have different sputtering rates.

A s a rule metallic alloy samples have a polycrystalline structure after solidification. Casting of commercial alloys even into a thin mould (with a cavity thickness of about 1 mm) produces a crystalline structure which is typical for metallic materials. Following the earlier works on rapidly solidified metallic glasses, a large number of metallic glassy alloys in the different alloy systems, including bulk glassy samples, have been produced in the past two decades by using various casting processes[1–5]. Physical vapor deposition methods are widely used to produce metallic glassy thin films. However, even by these methods, which have one of the highest available cooling rates, thin films with amorphous structure only of the certain chemical composition can be obtained[6].

Both Zr- and Pd-based alloys (Pd alloys being flux treated) are the best metallic glass-formers known up to date[7–9]. Zr-Pd system alloys were used to produce thin metallic glassy ribbon samples ($\sim$20 µm thick) by melt spinning. The formation of a primary nanoquasicrystalline phase was observed in Zr-rich area on heating[10,11]. It was shown that local atomic structure of the $Zr_{65}Pd_{35}$ glassy alloy is well described by taking into account the icosahedral atomic configuration[12]. It was also found that Zr_xPd_{1-x} (x = 0.59, 0,63, 0.67, and 0.70) amorphous alloys exhibit negative temperature coefficient of the resistivity between 10 and 300 K. These amorphous alloys also exhibit a transition to superconductive state at low temperatures[13].

Nanostructured metallic glasses or nanoglasses, consisting of irregularly placed spheroid glassy nanoparticles, represent a new and unique group of metallic materials with novel physical and chemical properties owing to their large surface area[14]. Metallic nano-glasses were first discovered several decades ago. Prof. Gleiter and his research group members fabricated nanoglasses by compaction of the spheroid nanoparticles produced by the inert gas condensation method[15]. Similar materials also can be produced by phase separation[16,17]. At certain conditions, individual metallic glassy particles of alloys[18] and even pure metals were also obtained[19]. Recently, nanostructured metallic glasses were also produced by magnetron sputtering[20]. It was found that Au-based[20] and Ti-based[21] nanoglasses have good catalytic activity and biocompatibility, respectively. Also $Fe_{90}Sc_{10}$ nanoglassy samples, unlike ribbon samples with a homogeneous glassy structure of the same chemical composition, exhibit ferro-magnetism at room temperature[22].

Both Zr and Pd are suitable constituent elements for biomaterials and Pd is also a good catalyst for certain chemical reactions. In the present paper we investigated the Zr-Pd amorphous thin films with nano-grained structure, prepared by magnetron sputtering technique. We also present their functional properties: resistance to corrosion and oxidation as well as their catalytic activity and biocompatibility.

Results

High catalytic activity of Pd in crystalline state is well known. Therefore, a glassy sample with high catalytic activity is presumed to contain as much Pd as possible. In present work, concentration of Zr in the sputtered films was varied from 10 to 46 at.%. X-ray diffraction patterns of the films with different Zr concentration are presented in Figure 1. As one can notice, only at 46 at.% of Zr (and above) the sputtered thin film becomes fully amorphous. However, further experiments on biocompatibility in the cell culturing solution revealed that, owing to the weak adhesion to the substrate, peaces of the nanoglass detached from the sample destroying osteoblasts. Therefore, in further experiments the compositions with lower palladium content were used. Also, according to the Pd-Zr phase diagram, higher Zr concentration leads to deeper eutectics and more stable glasses[23]. Finally, the nominal composition of 60 at.% Zr – 40 at. % Pd was chosen. Its X-ray diffraction pattern is shown in Figure 2.

According to the results of Gaussian fitting of the first diffraction maximum ranged from 35 to 46 degrees of 2θ in the X-ray diffraction pattern of the sputtered film (Figure 2) the center mass of the peak is located at $40.31 \pm 0.05°$. This value is not far from $37°$ of 2θ value obtained earlier for $Zr_{70}Pd_{30}$ glassy alloy prepared by melt spinning[10]. The difference is owing to somewhat higher Pd content in the sputtered alloy. This element, being smaller than Zr in size (Goldschmidt atomic radius of Zr is 160 pm while Pd has a size of 138 pm) causes a shift in the peak position[24]. High-resolution transmission electron microscopy and selected-area electron diffraction patterns also confirm amorphous nature of the sputtered films (Figure 2a,b).

The scanning electron microscopy (SEM) images obtained at different magnifications illustrate the granular morphology of the films (Figure 2c, d). The resulted composition measured by x-ray energy-dispersive analysis (EDX) installed in SEM over a large area of about 10^4 μm^2 was 62.5 ± 0.2 at.% Zr and 37.5 ± 0.2 at.% Pd. The average composition and confidence interval values were obtained as a result of five independent measurements. The difference with the intended composition could be due to the inhomogeneous distribution of the powder particles on the target surface and the difference in the sputtering yields of each component.

X-ray photoelectron spectroscopy (XPS) analysis of the as sputtered films surface revealed that the surface oxide film mostly consists of Zr atoms in 4 + oxidation state (Zr^0 peaks are very weak in Figure 3a). It is interesting to note that Pd^{2+} is also present in the surface oxide (Figure 3b) which indicates that Pd on the surface is also partially oxidized.

Thermal stability and oxidation behavior of the sputtered films were investigated. Isothermal annealing of the samples was carried out in the sputtering chamber, filled with dry air, right after the films preparation (temperature range: 100–500°C (373–773 K) for 1 hr (3.6 ks)). Analysis of the X-ray diffractometry (XRD) results (Figure 3c) revealed that annealing of the film in the temperature range of 100–300°C (373–573 K) does not lead to the formation of thick surface oxide and the surface retained its metallic color. Sharp peaks appeared in the XRD pattern only after annealing at 400°C (673 K). They were found to belong to the crystalline ZrO_2 (cubic symmetry, Pearson symbol cF12). The annealing at 500°C (773 K) caused formation of monoclinic mP12 ZrO_2 and tP4 PdO. Early crystallization stage of the metallic glassy matrix in dry air starts with the formation of the weak diffraction peak at $2\theta = 40.2°$ which may belong to the FCC Pd. Also, after annealing at 400°C (673 K) the color of the films surface changed from metallic to violet due to the oxidation, which is in agreement with the XRD results. One can also note that the XRD peaks, which belong to the ZrO_2 formed at 773 K, are significantly broader compared to those of the ZrO_2 formed at 673 K, which implies nanocrystallization of the surface oxide at 773 K. It should be noted here, that before in-situ annealing in the sputtering chamber for each annealing temperature an independent sample was prepared.

Corrosion behavior and chemical stability of the samples were studied in a simulated body fluid (Hank's solution, a water solution
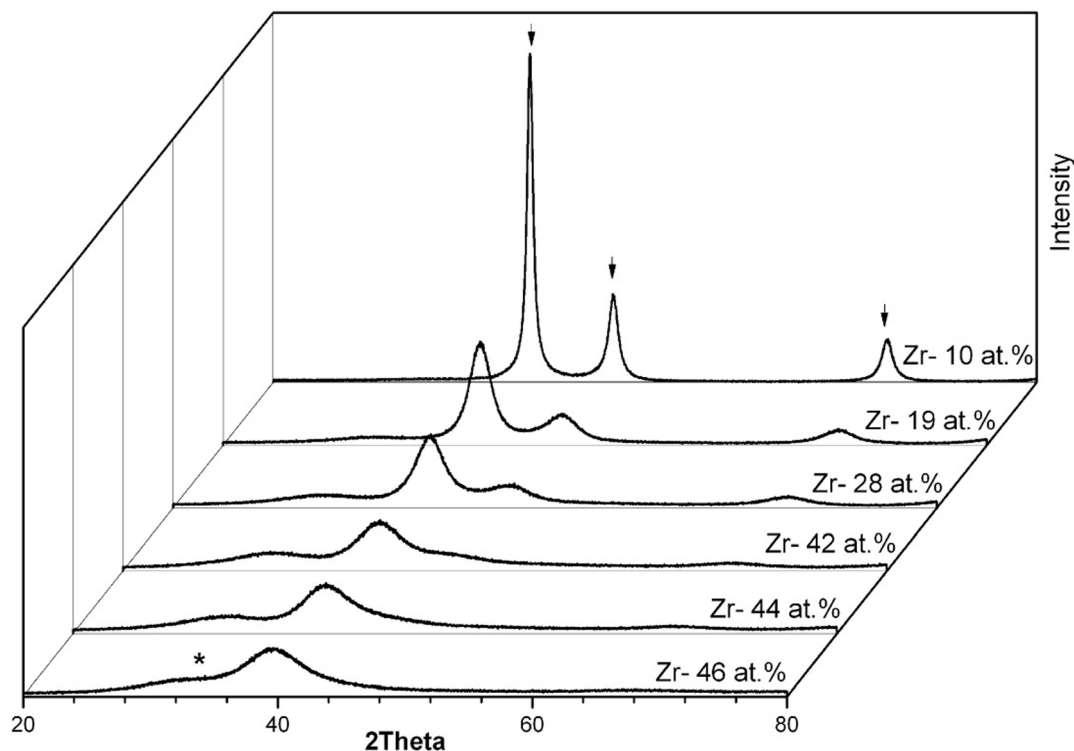
Figure 1 | X-ray diffraction patterns of the sputtered films with different concentration of Zr (Pd phase peaks are marked by arrows, while the star mark represents the broad peak from the substrate).
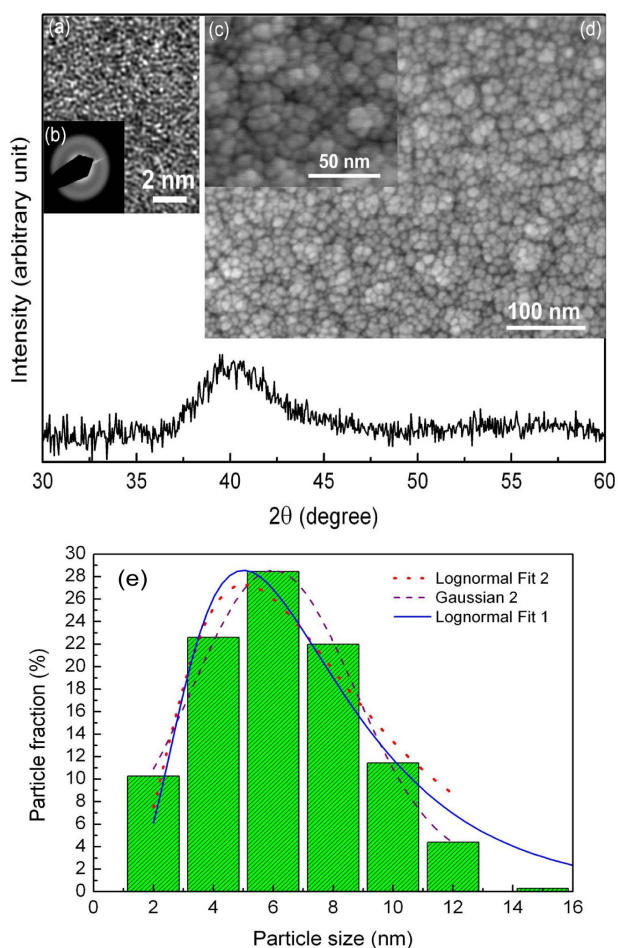
Figure 2 | **X-ray diffraction pattern of the sputtered film with 60 at.% of Zr.** The inserts (a) high-resolution transmission electron microscopy, (b) selected-area electron diffraction pattern and (c and d) SEM images obtained in secondary electrons at different magnification and (e) particles size distribution calculated from the SEM images (c) and three fits using Lognormal (full range and up to 12 nm size) and Gaussian (up to 12 nm size) function.

of naturally occurring salt body substances). The resulted polarization curve is presented on Figure 4. Anodic polarization of the sample is characterized by fairly rapid, within 300 s, establishment of a stationary potential (corrosion potential). As can be seen, during anodic polarization and transition to the passive state an activation peak is missing. This indicates self-passivation behavior related to the formation of a protective oxide film on the sample surface (mostly ZrO_2), as the second component of the alloy (Pd) is significantly more stable in the corrosive environment. Weak potential fluctuations ($\pm$ 2–3 mV) in the steady-state value (around 0 V) are associated with morphological features of the surface structure, and thus, the processes occurring on the alloys surface. These changes may be connected with the filling of the surface dips with the reaction products of the metal medium (here, likely, ZrO_2), which shields the metallic surface. Throughout the wide range of the potential, corresponding to the passive region (0–1000 mV), the alloy does not exhibit the pitting corrosion and metallic surface is preserved. The average current density in the passive state is low (for example, 3.5 mA/m^2 at 0.6 V and about 5.7 mA/m^2 at 1 V), which is an indicator of high corrosion resistance of the Zr-Pd film in such a corrosive biological environment.

Catalytic activity of the sputtered film was investigated in the Suzuki-coupling reaction. It was carried out after the electrolytic polishing in a solution of 900 ml of acetic acid with 100 ml per-

chloric acid (60%) at 15 V for 1 min to remove the oxide film. The reaction of 4-methylphenylboronic acid and iodobenzene was catalyzed by the material (0.16 mol% of Pd) at 50°C for 36 h and the desired 4-methylbiphenyl was obtained in 60% yield (Figure 5).This result clearly indicated that nanostructured Zr-Pd thin film, even with 40 at.% of Pd content, exhibits high catalytic activity for molecular transformations. The reaction products yield of about 60% is consistent with the reduced area of the sample after electrolytic polishing (see Methods section). It may be connected with the fact that some parts of the sample were etched out (Figure 6).

Osteoblast cells were chosen for biocompatibility test. These cells were deposited on the Zr-Pd nanoglassy films, which had pure Ti plate as substrate, and on the pure Ti sheet for comparison. The standard sample had a size of 10 $\times$ 10 mm. The purpose of the experiment was to evaluate the material's ability to induce cellular adhesion and proliferation. After 1 day of culture it was noticed that metallic glass surface exhibits more enhanced cellular growth and live/dead staining of the cells than pure Ti (Figure 7c,d). While on the day 7 the number of alive cells on both Ti and nanostructured metallic glass (MG) were statistically the same, on the day 14 this number on the MG sample became 14% higher. At this point most of the cells fused their borders and formed a connected net (figure 7d). For analysis of cytoskeleton organization and cell nucleus of the osteoblasts, grown on Ti and nanoglass, they were stained by TRITC–phalloidin and DAPI on Day 7 (Figure 7d). Osteoblasts formed well attached net to the surface on both Ti and Zr-Pd nanoglass. Following this, the activity of alkaline phosphatase (ALP) (an early marker for osteogenesis and an important enzyme produced by osteoblasts) and the secretion of osteocalcin (late osteogenic marker and the main noncollagenous protein associated with the formation of the mineralized matrix of bone in osteoblasts) were quantitatively determined (Figure 7a,b). During the whole cultivation period the difference of ALP activity and calcium secretion between nanoglass and pure Ti was minimal and statistically insignificant.

Discussion

Physical vapor deposition methods including the magnetron sputtering technique, having high cooling rates (higher then 10^8 K/s), are powerful tools to produce amorphous metallic thin films. However, even these methods do not always ensure formation of amorphous film. It may be partly connected with a relatively low deposition rate (about 110 pm/s) which allows surface diffusion to take place during deposition. In the present work, fully amorphous films were obtained only at high enough Zr content. In general, the obtained results correlate with the empirical rules introduced by Inoue[3]. In Pd-rich side the eutectic point is located at 40.1 at. % Zr, but only the films containing 46 at.% Zr or more were in amorphous state[23]. The deeper eutectic point at 25 at.% Pd content allowed to produce even more stable glassy film.

Thin films with an extremely fine glassy nano-granular structure (Figure 2c), as well as smooth thin films can be obtained via magnetron sputtering. Here we consider not individual glassy particles, but a material consisting of spheroid glassy particles connected by the glassy interfaces of the similar to the particle chemical composition. Fitting of the glassy particle size distribution (Figure 2e) with Lognormal distribution function (Lognormal Fit 1) gives the average size of about 6.5 nm (coefficient of determination $R^2 = 0.929$). If one removes the small fraction of the largest particles the (Lognormal Fit 2) the distribution becomes less well described ($R^2 = 0.887$), while the Gaussian fit produces the best fit ($R^2 = 0.998$) with the average particles size of 6 nm. These results indicate that real distribution is rather neither normal nor lognormal (right side part of the distribution is more steep compared to lognormal one), though both allowed to estimate the average particles size at 6–7 nm. Nevertheless, the absolute majority of the particles (99%) have a size ranging from 2 to 12 nm. At the same time, one can see that the sample
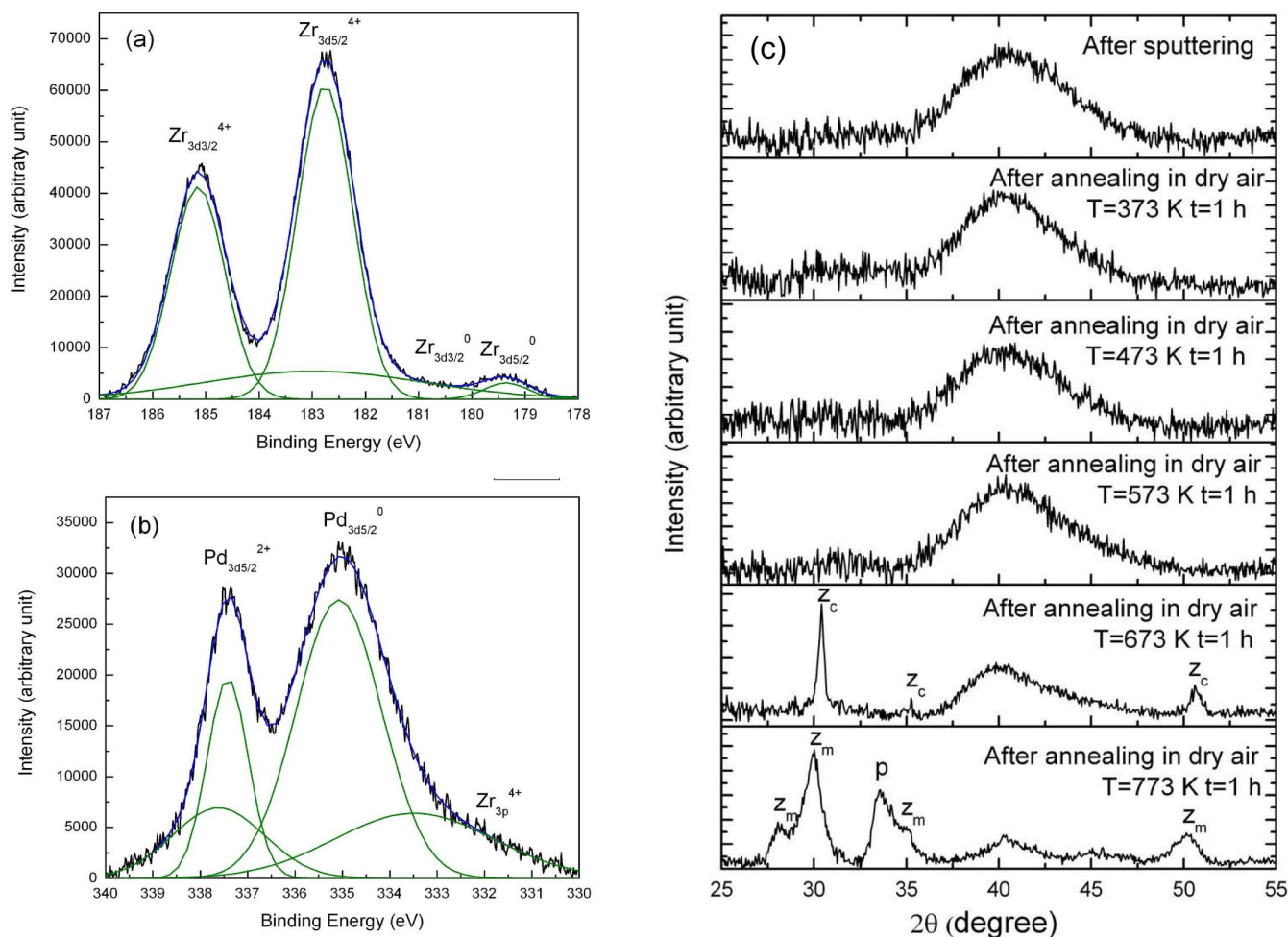
Figure 3 | XPS spectra related to (a) 3d Zr and (b) 3d Pd peaks of the as sputtered films surface layer and (c) x-ray diffraction patterns of the Zr-Pd thin films after annealing in dry air in the sputtering chamber. "z_c" and "z_m" denote the peaks of cubic and monoclinic ZrO_2 phases, respectively, while "p" indicates PdO phase.

has a hierarchical structure, where small particles below 12 nm in size are clustered, forming larger quasi-particles or columns which are roughly about 50 nm in size (see Figure 2c,d). Such a hierarchical (fractal-type) structure is known to be suitable for biomaterials[25]. Ti-Zr-Cu-Pd nano-structured metallic glass, having a similar structure, was recently tested as a coating for biomaterials, and found to be suitable for living cells attachment[20].
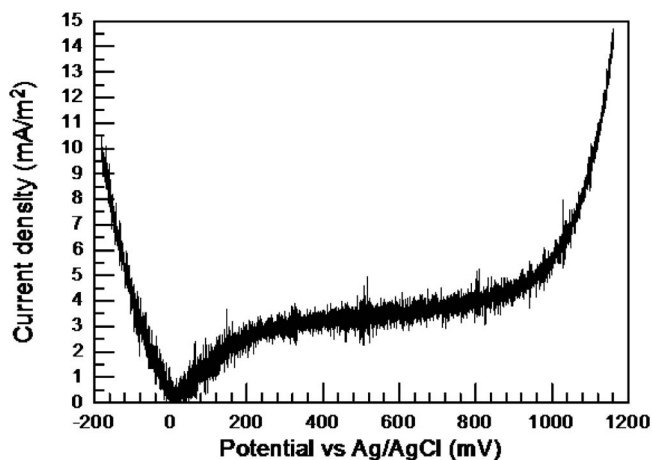

Figure 4 | Polarization curve measured in Hank's solution at 298 K.

High corrosion resistance of the Zr-Pd samples with extremely low current density of about 3.5 mA/m² (at 0.6 V) in a simulated body fluid provides compelling evidence that this nanostructured material can be applicable as a protective coating for biomaterials. Spontaneous passivation is achieved and low current density below 6 mA/m² maintains up to a very high potential of 1 V. This potential value is very high for metallic glasses and up to 1.1 V current density rise is very small (only about two times) while many other Zr-based metallic glasses studied earlier, exhibit a steep increase in the corrosion current after 0.5–0.6 V[26]. Obtained average current density value of about 3.5 mA/m² in the passivation region is very low for metallic alloys. Actual value per area should be even lower considering a non-smooth surface of the sample on the nanoscale (Figure 2c,d). The average current density value is lower than those values obtained for Ti-based[27–29], Zr-based[30,31] and Fe-based[26] glassy alloys as well as for crystalline alloys[32,33]

Zr as well as Ti forms a passive oxide layer. In addition, Zr ions show lower cell cytotoxicity than Ti[34] Moreover, the corrosion current density for pure Zr from its potentiodynamic polarization curve in Hank's solution at 0.3 V is about 15.3 μA/cm² which corresponds to 153 mA/m² and is significantly higher than that of the present nanostructured glassy alloy[35]

It was previously found that the addition of Pd to crystalline Zr decreases the passive current density. This indicates the stability of the passive film and decrease the amount of released metal ion at passive state[36]. Among the six pure metals investigated for in vitro
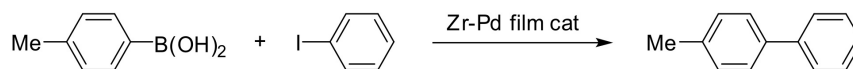
Figure 5 | Equation of chemical reaction, chosen for catalytic activity measurements.

cytotoxicity together with palladium alloys, Au, Pd and Ti were found to be the least cytotoxic, followed by Ag, then Ni, and finally Cu[37]. $Pd_{42.5}Cu_{30}Ni_{7.5}P_{20}$ bulk metallic glassy samples in Hanks' solution exhibited passive current densities of the order of 10^{-2}–10^{-1} A/m^2 (10–100 mA/m^2) in the anodic polarization curves[38], which are higher than those observed in the present Zr-Pd alloy.

Moreover, the investigation of the thermal stability and oxidation process of the nano-structured glassy samples showed that the present samples are steady against oxidation in a dry air up to 673 K while thermal crystallization of the glassy matrix is detected after annealing for 1 h at 773 K. This is consistent with the differential scanning calorimetry studies of the crystallization process in $Zr_{70}Pd_{30}$ and $Zr_{65}Pd_{35}$ glassy alloys studied earlier, which exhibited crystallization temperature of 727 and 771 K[10], respectively, at a heating rate of 0.67 K/s. Following the observed tendency, the present $Zr_{62.5}Pd_{37.5}$ nano-structured glassy alloy should have even higher crystallization temperature (T_x) at such a heating rate (T_x is the heating rate dependent). Moreover, an increase in the crystallization temperature of the nanoglassy samples was reported recently[39]. At 673 K only Zr severely oxidizes forming cubic form of ZrO_2 while at 773 K Zr forms the monoclinic form of ZrO_2 and even Pd starts to oxidize forming PdO (Figure 3c). This result is in consistence with oxidation of pure Pd performed at 823 K[40].

It was shown that melt-spun $Zr_{70}Pd_{30}$ monolithic glassy alloy samples underwent fast oxidation at 653 K in 30 min forming simultaneously two polymorphs of ZrO_2: tetragonal and monoclinic with underlying crystalline Pd[41]. Fast "catastrophic" oxidation of glassy $Zr_{70}Pd_{30}$ and $Zr_{70}Au_{30}$ was also observed and reported in Ref. 42. It was correlated with the formation of a lamellar structured scale consisting of the two phases, i.e. monoclinic and tetragonal ZrO_2, thus allowing fast oxygen diffusion. In addition, elements like Pd or Au found to accelerate the oxygen diffusivity in ZrO_2. Present results, however, indicate that nanostructured glassy films are quite stable up to 573 K.

XRD analysis of the annealed films revealed the existence of an untransformed metallic glassy phase underneath ZrO_2 even after annealing for 1 h at 673 K in dry air. Only at 773 K a minor fraction of a crystalline phase starts to form in the metallic glassy matrix. This finding allows us to anticipate that the nanostructured metallic glass is more stable against crystallization than the homogeneous one, produced by the melt spinning technique.
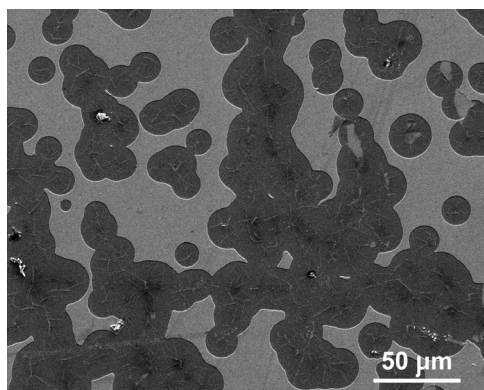
Figure 6 | SEM micrograph of a partial area of the sample after electrolytic polishing (secondary electrons). Dark dray areas were etched out while light gray areas represent the remaining sample.

After electrolytic polishing of the native surface oxide the sample exhibited a moderate catalytic activity in Suzuki-coupling reaction owing to the presence of a catalyst - Pd and nanostructured surface morphology of the sample with relatively large surface area. Earlier, such a behavior was also observed in de-alloyed nanoporous Pd-Ni-P metallic glassy sample[43]. Pd-Si metallic glasses were also applied earlier for a catalytic reaction[44].

Biocompatibility experiments also showed good results. Nanograined structure of the glassy film enhances the formation of the osteblast cells. Due to the modulated surface morphology and good corrosion resistance Zr-Pd nanostructured glassy films showed more enhanced cell growth ability than pure Ti but slightly lower ALP activity and calcium secretion. These results are similar to that reported for Ti-Zr-Cu-Pd nanoglass films[21]. However, a binary alloy with simpler composition was used in present work, which makes the target preparation process easier. Moreover, metallic glasses, in general, exhibit more enhanced mechanical properties and wear resistance than their crystalline counterparts[2,3]. The Zr-Pd biomaterial can also be suitable as a basis for biosensors and artificial tissue engineering.

In conclusion, among a wide range of Zr-Pd alloys studied fine nano-structured $Zr_{62.5}Pd_{37.5}$ metallic glassy thin film exhibits a good thermal stability versus crystallization and good resistance to oxidation in dry air up to 573–673 K. The samples also show a very high corrosion resistance and spontaneous passivation in a simulated body fluid. Spontaneous passivation leads to low current density, which maintains up to a very high potential of 1 V. The obtained current density of 3.5 mA/m^2 is a very low value for metallic alloys. After electrolytic polishing of native surface oxide the sample also exhibit catalytic activity in Suzuki-coupling reaction. Successful osteoblast cells cultivation on the nanoglassy surface indicates its good biocompatibility. Thus, this unique combination of physical and biochemical properties gives this material high application potential in biochemistry and implant engineering.

Methods

The thin Zr-Pd films were deposited on the oxide glass substrates containing 71.3 mass% SiO_2, 11 mass% Na_2O, 4.5 mass% K_2O, 7 mass% CaO, 1.5 mass% BaO, 0.7 mass% Al_2O_3, 4.2 mass% ZnO from elemental powder mixtures having purities over 99.9 mass% by using conventional Ar-gas carrier RF magnetron sputtering technique. The details are as follows: forward power: 70 W, the distance between the target and the sample: 70 mm, background argon pressure: 2 Pa, initial pressure: 2–4×10^{-4} Pa, argon flow: 10 ml/min and the average deposition rate of about 110 pm/s. The average particle size of the elemental crystalline powders mixed homogeneously in the target used for sample preparation was about 10 µm. Different compositions were obtained by the different volume ratio of Pd and Zr powders in the mixture.

When necessary, the oxidation annealing of the samples was preformed in the same sputtering chamber in the dry mixture of nitrogen (79%) and oxygen (21%) to avoid any unnecessary reactions with water. Oxidation was carried out isothermally in the temperature interval 100–500°C (373–773 K) for 1 hr (3.6 ks). Each time an original sample was sputtered.

The structure and surface morphology of the thin films were investigated by X-ray diffractometry (XRD) using Cu K_α radiation and scanning electron microscopy (SEM) methods, respectively. The elemental composition analysis was conducted by the energy dispersive X-ray (EDX) spectroscopy device attached to the scanning electron microscope. Transmission electron microscopy (TEM) investigations were carried out using a microscope operating at 200 kV. The samples for TEM were prepared by an ion polishing technique. In order to avoid structural damage the ion-beam energy was kept as low as 2 keV. X-ray photoelectron spectroscopy (XPS) was carried out using an apparatus equipped with Scienta MX650 X-ray source of 0.2 kW power having the Al Kα (1486.7 eV) radiation.

Electrochemical measurements were performed on an electronic potentiostat, which enables continuous automatic recording of the electrochemical parameters with potential sweep rate of 0.2 mV/s. The electrochemical measurements were conducted in a three-electrode cell using a platinum counter-electrode and an Ag/AgCl reference electrode. The potentiodynamic polarization curves were measured at
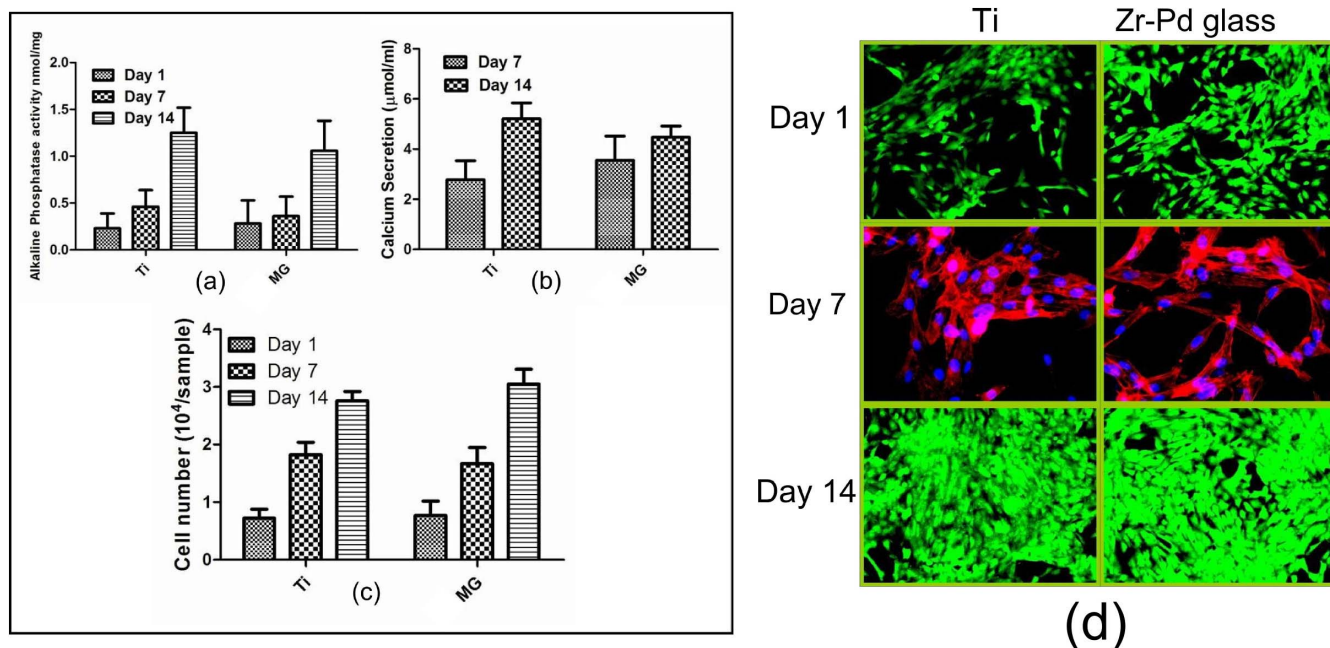
Figure 7 | Alkaline phosphatase activity (a), calcium secretion (b), proliferation (c) and live/dead staining of cells (d) cultured on Ti and metallic glass (MG) (Day 1, Day 14), Day 7 - merged photos of F-actin (red) and nuclei (blue) staining of cells cultured on Ti and MG for 7 days.

25°C (298 K) in the Hank's solution of 8 NaCl, 0.4 KCl, 0.12 $Na_2HPO_4\cdot12H_2O$, 0.06 KH_2PO_4, 0.2 $MgSO_4\cdot7H_2O$, 0.35 $NaHCO_3$, 0.14 $CaCl_2$, H_2O (up to 1 liter); pH = 7.4 when the open-circuit potential became almost steady[44–46]. Before recording the polarization curve the sample was treated at a potential of 180 mV to remove any surface contamination.

Suzuki coupling reaction was also carried out in the presence of the Zr-Pd material as a catalyst[47]. In order to clean the surface, electrolytic polishing was conducted in 900 ml of acetic acid with the 100 ml perchloric acid (60%) at 10 V for 1 min. After washing in pure water and methanol, the material (0.22 mg, 0.16 mol% Pd) was added to a solution of potassium hydroxide (140 mg, 2.5 mmol) in methanol (2 ml) at room temperature. Later 4-Methylphenylboronic acid (102 mg, 0.75 mmol) and iodobenzene (55.7 ml, 0.5 mmol) were added to the mixture, and stirred at 50°C for 36 h. After cooling, Ethyl acetate (EtOAc) was added and the liquid moiety was washed in water and brined in the separation funnel. The organic layer was evaporated to leave the crude product, which was purified by silica gel column chromatography with hexane. The yield was calculated on the basis of the weight of the isolated product and depends on the surface area of the catalyst.

Osteoblasts (from American Type Culture Collection, Passage 7) were maintained in Eagle's medium (MEM) with 10% (v/v) fetal bovine serum (FBS) and 1% penicillin/streptomycin. Typically, 100 µl cell suspensions (1×10^6 cells per ml) were seeded onto the surfaces of Zr-Pd or Ti films (1 cm × 1 cm) and cultured for 14 days. After 1 day, 7 days and 14 days of culture, the cell number was determined using cell counting kit-8 (Sigma-Aldrich, USA) following the manufacturer's instructions. Nuclei were counterstained with DAPI (Invitrogen, USA) and F-actin was stained with TRITC–phalloidin. A Live/Dead kit (Invitrogen, USA) was used to distinguish between live and dead cells. After staining by this kit, the live and dead cells exhibited green and red color, respectively.

Alkaline phosphatase (ALP) activity of osteoblasts was performed via pNPP assay (p-nitrophenyl phosphate liquid substrate, Sigma-Aldrich, USA). Briefly, cells on the Zr-Pd or Ti films were lysed in 0.1% Triton X-100 solutions for 10 min at 4°C. After adding pNPP into the lysate, the mixed solution was incubated at 37°C for 30 min, and the absorbance at 405 nm of the solution was measured by a plate reader (BioTex, USA). Finally, ALP activity was calculated via a formula given by the manufacturer after normalizing the cell number[48,49]. Osteocalcin levels of the cells on the patterns were tested using an Osteocalcin direct ELISA kit (Invitrogen, USA) following the manufacturer's instructions. The calcium secretion of cells were measured using Calcium Colorimetric assay kit (Sigma-Aldrich, US).

1. Klement, W., Willens, R. H. & Duwez, P. Non-crystalline Structure in Solidified Gold–Silicon Alloys. *Nature* **187**, 869–870 (1960).
2. Inoue, A. High Strength Bulk Amorphous Alloys with Low Critical Cooling Rates. *Mater. Trans. JIM* **36**, 866 (1995).
3. Inoue, A. Stabilization of metallic supercooled liquid and bulk amorphous alloys. *Acta Mater.* **48**, 279–306 (2000).
4. Johnson, W. L. Bulk Glass-Forming Metallic Alloys: Science and Technology. *MRS Bull.* **24**, 42–56 (1999).
5. Egami, T. Nano-glass Mechanism of Bulk Metallic Glass Formation. *Mater. Trans.* **43**, 510–517 (2002).
6. Louzguine-Luzgin, D. V., Ketov, S. V., Orava, J. & Mizukami, S. Optically transparent magnetic and electrically conductive Fe–Cr–Zr ultra-thin films. *Phys. Status Solidi A* **211**, 999–1004 (2014).
7. Nishiyama, N. & Inoue, A. Glass-Forming Ability of Bulk $Pd_{40}Ni_{10}Cu_{30}P_{20}$ Alloy. *Mater Trans JIM* **37**, 1531–1539 (1996).
8. Lu, I.-R., Wilde, G., Görler, G. P. & Willnecker, R. Thermodynamic properties of Pd-based glass-forming alloys. *J. Non-Cryst. Solids* **250–252**, 577–581 (1999).
9. Chen, N. *et al.* Flux-induced structural modification and phase transformations in a $Pd_{40}Ni_{40}Si_4P_{16}$ bulk-glassy alloy. *Acta Mater.* **58**, 5886–5897 (2010).
10. Murty, B. S., Ping, D. H. & Hono, K. Nanoquasicrystallization of binary Zr-Pd metallic glasses. *Appl.Phys. Let.* **77**, 1102–1104 (2000).
11. Kramer, M. J. *et al.* Devitrification studies of Zr-Pd and Zr-Pd-Cu metallic glasses. *J. of Non-Cryst. Solids* **317**, 62–70 (2003).
12. Takahara, Y. & Narita, N. Local Electronic Structures and Chemical Bonds in Zr-Based Metallic Glasses. *Mater. Trans.* **45**, 1172–1176 (2004).
13. Gruzalski, G. R., Gerber, J. A. & Sellmyer, D. J. Electronic properties and superconductivity of Zr-Pd glasses. *Phys. Rev. B* **19**, 3469–3475 (1979).
14. Gleiter, H., Schimmel, Th & Hahn, H. Nanostructured solids — From nano-glasses to quantum transistors. *Nano Today* **9**, 17–68 (2014).
15. Fang, J. X. *et al.* Atomic structure and structural stability of $Sc_{75}Fe_{25}$ nanoglasses. *Nano Lett.* **12**, 458–463 (2012).
16. He, J. H., Sheng, H. W., Schilling, P. J., Chien, C.-L. & Ma, E. Amorphous Structures in the Immiscible Ag-Ni System. *Phys. Rev. Let.* **86**, 2826 (2001).
17. Banerjee, R., Puthucode, A., Bose, S. & Ayyub, P. Nanoscale phase separation in amorphous immiscible copper-niobium alloy thin films. *Appl. Phys. Let.* **90**, 021904 (2007).
18. Jing, J., Kramer, A., Birringer, R., Gleiter, H. & Gonser, U. Modified atomic structure in a PdFeSi nanoglass. A Mössbauer study. *J. Non-Cryst. Solids* **113**, 167–170 (1989).
19. Kim, Y.-W., Lin, H.-M. & Kelly, T. F. Amorphous solidification of pure metals in submicron spheres, *Acta Metall.* **37**, 247–255 (1989).
20. Chen, N. *et al.* Formation and properties of Au-based nanograined metallic glasses *Acta Mater.* **59**, 6433–6440 (2011).
21. Chen, N. *et al.* A novel Ti-based nanoglass composite with submicron–nanometer-sized hierarchical structures to modulate osteoblast behaviors. *J. Mater. Chem. B* **1**, 2568–2574 (2013).
22. Witte, R. *et al.* Evidence for enhanced ferromagnetism in an iron-based nanoglass. *Appl. Phys. Let.* **103**, 073106 (2013).
23. Okamoto, H. Pd-Zr (Palladium-Zirconium). *J. of Phase Equilibria and Diffusion* **30**, 413–414 (2009).
24. Gale, W. F. & Totemeier, T. C. *Smithells Metals Reference Book* [8-th ed], (Elsevier Butterworth-Heinemann Ltd., Oxford, 2004).
25. Tan, J. & Saltzman, W. M. Biomaterials with hierarchically defined micro- and nanoscale structure. *Biomaterials* **25**, 3593–3601 (2004).
26. Wang, Y. B., Li, H. F., Zheng, Y. F. & Li, M. Corrosion performances in simulated body fluids and cytotoxicity evaluation of Fe-based bulk metallic glasses. *Mater. Sci. and Eng. C* **32**, 599 (2012).

27. Oak, J. J., Louzguine-Luzgin, D. V. & Inoue, A. Fabrication of Ni-free Ti-based bulk-metallic glassy alloy having potential for application as biomaterial, and investigation of its mechanical properties, corrosion, and crystallization behavior. *J. of Mater. Res.* **22**, 1346–1353 (2007).

28. Qin, F. *et al.* Corrosion Behavior of a Ti-Based Bulk Metallic Glass and Its Crystalline Alloys. *Mater. Trans.* **48**, 1855–1858 (2007).

29. Oak, J. J., Louzguine-Luzgin, D. V. & Inoue, A. Investigation of glass-forming ability, deformation and corrosion behavior of Ni-free Ti-based BMG alloys designed for application as dental implants. *Mater. Sci. and Eng.: C* **29**, 322–330 (2009).

30. Wang, Y. B., Zheng, Y. F., Wei, S. C. & Li, M. In vitro study on Zr-based bulk metallic glasses as potential biomaterials. *J. of Biomed. Mater. Res. B: Appl. Biomater.* **96B**, 34–46 (2011).

31. Qiu, C. L. *et al.* A novel Ni-free Zr-based bulk metallic glass with enhanced plasticity and good biocompatibility. *Scripta Mater.* **55**, 605–608 (2006).

32. Lavos-Valereto, I. C., Wolynec, S., Ramires, I., Guastaldi, A. C. & Costa, I. Electrochemical impedance spectroscopy characterization of passive film formed on implant Ti-6Al-7Nb alloy in Hank's solution. *J. of Mater. Sci.: Mater. in Medic.* **15**, 55–59 (2004).

33. Sridhar, T. M., Kamachi, M. U. & Subbaiyan, M. Preparation and characterisation of electrophoretically deposited hydroxyapatite coatings on type 316L stainless steel. *Corrosion Sci.* **45**, 237–252 (2003).

34. Yamamoto, A., Honma, R. & Sumita, M. Cytotoxicity evaluation of 43 metal salts using murine fibroblasts and osteoblastic cells. *J. Biomed. Mater. Res.* **39**, 331–340 (1998).

35. Zhou, F. Y. *et al.* Microstructure, corrosion behavior and cytotoxicity of Zr–Nb alloys for biomedical application. *Mater. Sci. and Eng. C* **32**, 851–856 (2012).

36. Tsutsumi, Y., Takano, Y., Doi, H., Noda, K. & Hanawa, T. Corrosion behavior of Zr-Pt and Zr-Pd alloys for biomaterials in simulated body fluid. *Paper presented at 214th Meeting of the Electrochemical Society. Fall Meeting of The Electrochemical Society of Japan PRiME, Honolulu, The Electrochemical Society*, (2008) *October 12–17*.

37. Craig, R. G. & Hanks, C. T. Cytotoxicity of experimental casting alloys evaluated by cell culture tests. *J. Dent. Res.* **69**, 1539–1542 (1990).

38. Qin, F., Xie, G., Wada, T., Zhu, S. & Dan, Z. Electrochemical Properties of Porous Pd-Based Bulk Metallic Glasses. *Mater. Trans.* **54**, 1347–1350 (2013).

39. Wang, J. Q., Chen, N., Glendenning, T. W., Louzguine, D. V. & Perepezko, J. H. The thermal behavior of a nano-grained Au-based glass. *Paper presented at 20th International Symposium on Metastable and Nano Materials (ISMANAM-2013)*. Book of Abstracts. *Torino, Italy, 2013, June 30-July 5.*

40. Pilloy, Th., Zimmermann, R., Steiner, P. & Hufner, S. The electronic structure of PdO found by photoemission (UPS and XPS) and inverse photoemission (BIS). *J. Phys.: Condens. Matter* **9**, 3987–3999 (1997).

41. Mondal, K., Chatterjee, U. K. & Murty, B. S. Oxidation behavior of amorphous and nanoquasicrystalline Zr–Pd and Zr–Pt alloys. *J. of Alloys and Compd.* **460**, 172–181 (2008).

42. Köster, U. & Jastrow, L. Oxidation of Zr-based metallic glasses and nanocrystalline alloys. *Mater. Sci. Eng. A* **449–451**, 57–62 (2007).

43. Tanaka, S. *et al.* A nanostructured skeleton catalyst: Suzuki-coupling with a reusable and sustainable nanoporous metallic glass Pd-catalys. *Chem. Commun.* **47**, 5985–5987 (2011).

44. Molnár, Á., Smith, G. V. & Bartók, M. Hydrogenation of (+)-Apopinene over Pd-Si and Pd-Ge Glasses. *J. of Catalysis* **101**, 540–544 (1986).

45. de Assis, S. L., Wolynec, S. & Costa, I. Corrosion characterization of titanium alloys by electrochemical techniques. *Electrochimica Acta* **51**, 1815–1819 (2006).

46. ASTM Standard G59-97 ″Standard Test Method for Conducting Potentiodynamic Polarization Resistance Measurements″ *Annual Book of ASTM Standards* [Volume 03.02] (ASTM International, West Conshohocken, PA, 2014).

47. Miyaura, N., Suzuki, A. Stereoselective synthesis of arylated (E)-alkenes by the reaction of alk-1-enylboranes with aryl halides in the presence of palladium catalyst. *Chem. Comm.* **19**, 866–867 (1979).

48. Shi, X. T. *et al.* Microsphere-based drug releasing scaffolds for inducing osteogenesis of human mesenchymal stem cells in vitro. *Eur. J. Pharm. Sci.* **39**, 59–67 (2010).

49. Shi, X. T. *et al.* In-vitro osteogenesis of synovium stem cells induced by controlled release of bisphosphate additives from microspherical mesoporous silica composite. *Biomaterials* **30**, 3996–4005 (2009).

Acknowledgments

Author contributions

S.V.K. and D.V.L.-L. wrote and corrected the manuscript text and figures, X.T. Sh. and H.W. prepared fig. 6 and wrote the biocompatibility part, G.X. and R.K. prepared fig. 3 and wrote XPS measurement part, A. Yu. Ch., A.I.B. and N. Ch. prepared fig. 4 and wrote corrosion testing part, Y.I. and N.A. prepared fig. 5 and wrote catalytic activity part. All authors reviewed the manuscript.

Additional information